ELSEVIER

Thermochimica Acta 337 (1999) 219–226

thermochimica acta

www.elsevier.com/locate/tca

Heat transfer modeling of a DSC plate transducer

A. Lindemann, J. Schmidt*

Otto von Guericke University, Institut für Strömungstechnik und Thermodynamik, Abt. Thermodynamik, Universitätsplatz 2, D-391 06 Magdeburg, Germany

Received 11 May 1999; accepted 4 June 1999

Abstract

A model is presented which describes the heat transfer between the subsystems of a DSC plate transducer. For the modeling, the DSC plate transducer is divided into seven subsystems with locally uniform temperature. The simulation program for the solution of the model equations is based on the Runge–Kutta–Fehlberg method. Appropriate planning of the experiments can be derived as a result. Thus, the expense of the preliminary experiments can be reduced. In addition, the model allows the measured results to be interpreted more easily.

Keywords: Differential scanning calorimetry; Simulation; Model; Plate; Transducer; DSC

1. Introduction

DSC measurements for the determination of the specific heat capacity require a high measuring accuracy and good reproducibility. In [1] the possibilities for the improvement of the signal to noise ratio were discussed. In particular, a sensitive influence of the DSC signal occurs by the measuring conditions within the high temperature range. Appropriate planing of the measurements, e.g. for the selection of the crucibles and the reference material, the definition of the dimensions of sample and reference specimen, selection of the temperature program and the selection of the sweep gas mostly require many preliminary experiments with variation of the parameters. This approach is expensive and time consuming. In addition, it is often difficult to interpret realistically the measured results in connection with the influences of the measuring conditions. For these reasons modeling of the heat transfer with consideration of thermal conduction, convection and radiation is presented. The aims are simplified modeling on the basis of a system of ordinary differential equations, the simulation of the DSC signal in dependency on the essential measuring conditions and the evaluation of the different factors of influence on the measuring signal and the selection of appropriate experimental conditions. Similar models for the temperature-modulated differential scanning calorimetry (TMDSC) were already presented in [2,3], and [4,5] gives some indication of the interpretation of DSC signals.

2. Model

The DSC plate transducer DSC92 (SETARAM) with reference and sample crucible (platinum) is

*Corresponding author. Tel.: +49-391-67-18575; fax: +49-391-67-12762

E-mail address: juergen.schmidt@vst.uni-magdeburg.de (J. Schmidt)

0040-6031/99/$ – see front matter
PII: S0040-6031(99)00167-7

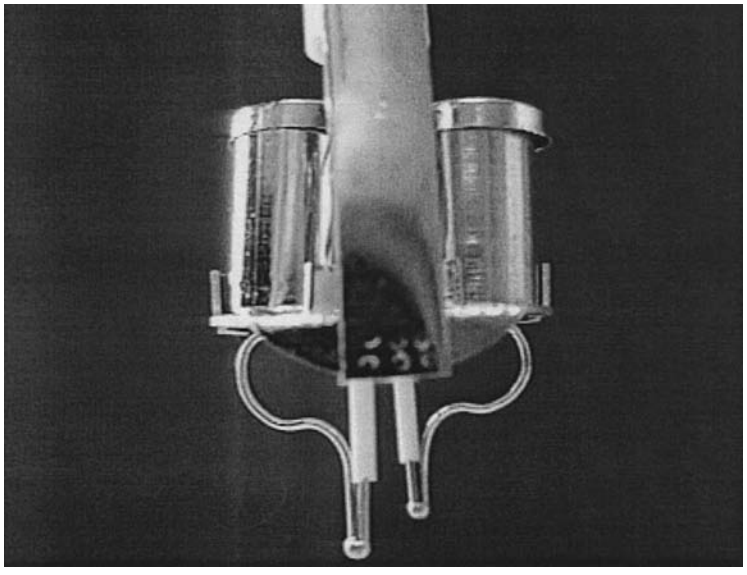

Fig. 1. DSC plate transducer D5C92 (SETARAM) with reference and sample crucibles (platinum).

shown in Fig. 1. The temperature difference between sample side and reference side, which corresponds to the DSC signal, is directly measured by thermocouples on the DSC plate. For the modeling, the DSC plate transducer is divided into seven subsystems with locally uniform temperature $T_i(t)$, Fig. 2.The assumption of a homogeneous temperature of the subsystems at each point in time is equivalent to the assumption of $\mathrm{Bi} \to 0$ in transient heat conduction problems. The Biot number

$$\mathrm{Bi} = \frac{\alpha \cdot l_{\mathrm{char}}}{\lambda} = \frac{l_{\mathrm{char}}/\lambda}{1/\alpha}, \tag{1}$$

characterizes the relation of the internal resistance of the heat conduction to the outside thermal resistance. In most practical applications the thermal resistance

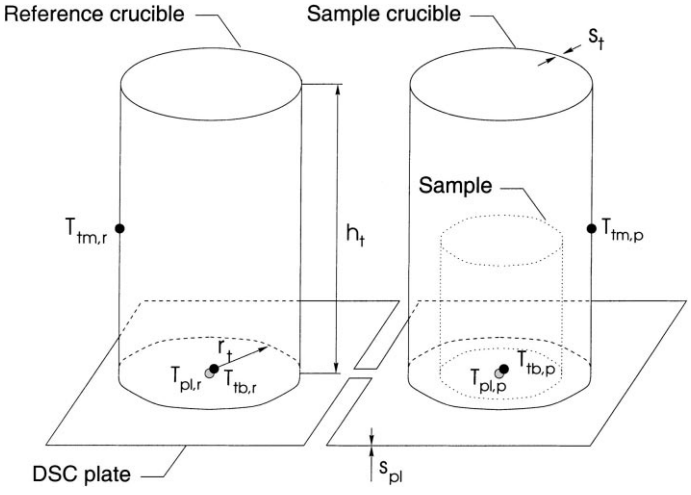

Fig. 2. Sketch of the subsystems involved in the heat transfer.

can be neglected without a loss of accuracy for $Bi \leq 0.1$. This assumption can be verified by solution of the Fourier differential equation.

In addition, the following assumptions are made:

formulation of the heat flows between the subsystems on the basis of thermal resistances R_i^j and simplifying assumptions,
symmetric conditions for the sample and reference side ($\Rightarrow$ horizontal base line),
heat transfer between the subsystems by thermal conduction, convection and radiation.

During heating and cooling, the temperatures T_i of the subsystems differ and heat flows

$$\dot{Q}_{ij} = A_i(T_i - T_j)/R_i^j \tag{2}$$

appear. Thermal resistances R_i^j are modeled for the simulation of the heat transfer between the subsystems i and j with consideration of thermal conduction, convection and radiation.

In particular, within the high temperature range (>1000°C) the heat transfer by radiation gains in importance e.g., the radiation plays a crucial role between the furnace wall and the respective crucible coat, the inside surface of the crucible and the sample, the outside surfaces of both crucibles as well as between the plate of the DSC and the colder zones of the furnace. The latter can be also a cause for the intensified drift of the base line in the high temperature range as a result of asymmetry if no sufficient radiation protection is installed in the measuring field.

The thermal resistance between furnace wall (o) and crucible coat (tm) can be formulated for example as follows:

$$R_{tm}^{o} = \left(\varepsilon_{tm} \cdot \sigma_s \cdot \frac{T_o^4 - T_{tm}^4}{T_o - T_{tm}} + \alpha_{conv} \right)^{-1}. \tag{3}$$

The radiation is considered according to the law of Stefan and Boltzmann. The heat transfer coefficient α_{conv} is used for the consideration of convective heat transfer. For the estimation of α_{conv} the heat transfer coefficient for the laminar heat transfer in a gap with the effective gap width s_{eff} is used [6]:

$$\begin{aligned} Nu \geq Nu_{min} \text{ (full development flow)} \\ = 4.96 = \frac{\alpha \cdot 2 s_{eff}}{\lambda(T_o)}, \end{aligned} \tag{4}$$

$$\alpha_{conv,min}(T_o) = \frac{4.86}{2 s_{eff}} \cdot \lambda_{gas}(T_o). \tag{5}$$

Due to the thermal and hydrodynamic development of the flow, the real heat transfer coefficient is higher

$$\alpha_{conv}(T_o, \dot{V}_{gas}) \geq \alpha_{conv,min}. \tag{6}$$

This depends in particular on the furnace temperature and the adjusted flow rate of the sweep gas $\dot{V}_{gas}$.

The general formulation of the resistance considering heat conduction and the contact resistance between two bounding subsystems, reads as:

$$R_{i,HC}^j(T) = \frac{s_i}{2\lambda_i(T_o)} + \frac{s_j}{2\lambda_j(T_o)} \frac{s_{rough,eq}}{\lambda_{gas}(T_o)}, \tag{7}$$

where λ_i represents the thermal conductivity. s_i is the dimension of the subsystem which is characteristic for the heat conduction. The term $s_{rough,eq}/\lambda_{gas}(T_o)$ describe the thermal resistance at the interface of the two subsystems (e.g. sample–crucible ground, crucible ground–DSC plate). This depends on the thermal conductivity λ of the sweep gas (e.g. $\lambda_{He} \approx 9\lambda_{Ar}$) and on the surface quality of the sample and the crucible. The latter is considered by an equivalent gas layer thickness $s_{rough,eq}$, which has the same resistance against heat conduction as the contact zone formed by the roughness and the gas gaps. So a good description of the temperature dependence of the contact resistance can be also achieved. By varying the equivalent roughness $s_{rough,eq}$ in the calculations, conclusions can be derived about the influence of the surface quality of the sample or the reference material. The influence of the sweep gas on the contact resistance can be simulated based on the variation of the thermal conductivity λ_{gas}.

The model is based on a system of ordinary differential equations with one differential equation per subsystem. Depending on the temperature program or the heating rate $\beta(t)$, the rate of change of the furnace temperature can be expressed as follows

$$\frac{dT_o}{dt} = \beta(t). \tag{8}$$

The application of the first law of thermodynamics for rigid systems with exclusive heat transfer

$$dU = dQ = \dot{Q}dt \tag{9}$$

to the respective subsystems leads to the following differential equations: reference side of DSC plate transducer

$$(mc)_{tm,r}\frac{dT_{tm,r}}{dt}=\frac{A_{tm}}{R^{o}_{tm,r}}(T_o-T_{tm,r})+\frac{A_{q,tm}}{R^{tb,r}_{tm,r}}(T_{tb,r}-T_{tm,r})+\frac{A_{tm}}{R^{tm,p}_{tm,r}}(T_{tm,p}-T_{tm,r}), \quad (10)$$

$$(mc)_{tb,r}\frac{dT_{tb,r}}{dt}=\frac{A_{q,tm}}{R^{tb,r}_{tm,r}}(T_{tm,r}-T_{tb,r})+\frac{A_{tb}}{R^{pl,r}_{tb,r}}(T_{pl,r}-T_{tb,r}), \quad (11)$$

$$(mc)_{pl,r}\frac{dT_{pl,r}}{dt}=\frac{A_{tb}}{R^{pl,r}_{tb,r}}(T_{tb,r}-T_{pl,r})+\frac{A_{q,pl}}{R^{pl,p}_{pl,r}}(T_{pl,p}-T_{pl,r})+\frac{A_{pl}}{R^{o}_{pl,r}}(T_o-T_{pl,r}), \quad (12)$$

$$(mc)_{tm,p}\frac{dT_{tm,p}}{dt}=\frac{A_{tm}}{R^{o}_{tm,p}}(T_o-T_{tm,p})+\frac{A_{q,tm}}{R^{tb,p}_{tm,p}}(T_{tb,p}-T_{tm,p})+\frac{A_{tm}}{R^{tm,p}_{tm,r}}(T_{tm,r}-T_{tm,p})+\frac{A_{tm}}{R^{pr}_{tm,p}}(T_{pr}-T_{tm,p}), \quad (13)$$

$$(mc)_{tb,p}\frac{dT_{tb,p}}{dt}=\frac{A_{q,tm}}{R^{tb,p}_{tm,p}}(T_{tm,p}-T_{tb,p})+\frac{A_{tb}}{R^{pl,p}_{tb,p}}(T_{pl,p}-T_{tb,p})+\frac{A_{q,pr}}{R^{pr}_{tb,p}}(T_{pr}-T_{tb,p}), \quad (14)$$

$$(mc)_{pl,p}\frac{dT_{pl,p}}{dt}=\frac{A_{tb}}{R^{pl,p}_{tb,p}}(T_{tb,p}-T_{pl,p})+\frac{A_{q,pl}}{R^{pl,p}_{pl,r}}(T_{pl,r}-T_{pl,p})+\frac{A_{pl}}{R^{o}_{pl,p}}(T_o-T_{pl,p}), \quad (15)$$

$$(mc)_{pr}\frac{dT_{pr}}{dt}=\frac{A_{tm}}{R^{pr}_{tm,p}}(T_{tm,p}-T_{pr})+\frac{A_{q,pr}}{R^{pr}_{tb,p}}(T_{tb,p}-T_{pr}). \quad (16)$$

The numerical solution of the system of differential equations was carried out by means of the Runge–Kutta–Fehlberg method with an estimation of the local error as well as an automatic control of the step size [7]. A test of the program and a prediction of the maximum step size Δt_{max} was done on the basis of analytical solutions. This results in a stable and robust solution algorithm, which allows simulation calculations.

3. Results

A temperature program within the range of 700–1400°C was used to demonstrate the efficiency of the model. The comparison of the measured DSC signal with the simulation was carried out on this basis. The heating rate between the plateaus with a temperature difference of 100 K was 5 K/min. Helium was used as the sweep gas. In order to allow comparisons between different materials, platinum and Al_2O_3 crucibles as well as a platinum sample cylinder were used.

3.1. Behavior of the subsystems in dependency on the time

Assuming ideal conditions, a temperature compensation between the subsystems of the DSC plate transducer continues until steady-state takes place if the furnace temperature is kept constant (plateau). This thermal equilibrium is disturbed by the beginning of the heating. A quasi-steady-state will be reached again if the rate of heating is constant. The temperature of the subsystem considered follows the given furnace temperature in dependency on the thermal resistances and the heat capacity, as shown in Fig. 3. The simulated temperature distribution of the subsystems for the transition from a plateau to a constant heating rate are presented as an example for selected experimental conditions. It is evident that the temperatures of the subsystems on the reference side correspond better to the furnace temperature than temperatures of the appropriate subsystems on the

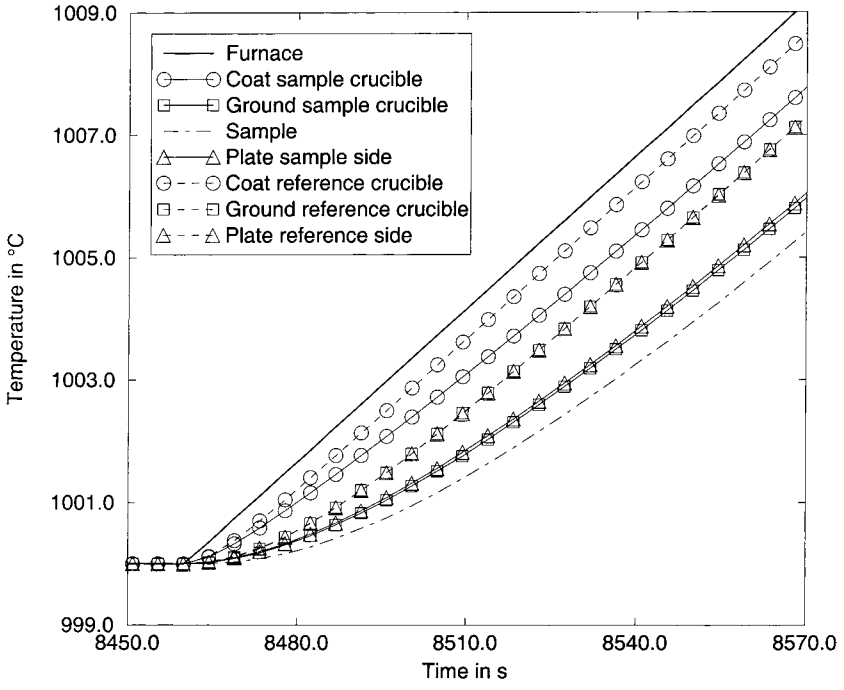

Fig. 3. Presentation of the simulated temperature distribution of the subsystems for the transition from a plateau (T_o=1000°C) to a constant heating rate (β = 5 K/min).

sample side. In comparison to the reference side, the subsystems of the sample side additionally transfer heat to the sample which leads to a temperature decrease. For example, the crucible coat temperatures correspond better to the furnace temperature than the temperatures of the crucible ground or the sample. This is caused by the direct heat exchange between the outside surfaces of the crucibles and the furnace. The temperature of the DSC plate equals approximately the temperature of the corresponding crucible ground. The reason for that is a slight heat conduction resistance between plate and crucible ground. This resistance depends on the surface quality of the crucibles and of the plate and the thermal conductivity of the sweep gas. Similar connections result for the temperature of the sample.

The comparison with the experiment shows that no thermal equilibrium can be achieved under real conditions, even with constant furnace temperature (plateau). The temperatures of the subsystems differ also in the steady-state from the furnace temperature, because a heat transfer from the DSC plate transducer to the colder area of the equipment occurs.

3.2. Influence of the crucible material

With rising temperature the influence of the radiation between the subsystems increases. Especially in the high temperature range it is essential which type of crucible material is used. Fig. 4 shows the crucibles available for DSC measurements. The reasons for the use of platinum crucibles instead of $A1_2O_3$ crucibles are the smaller radiation coefficient, the better thermal conductivity of platinum and the smaller contact resistance. However, platinum crucibles cannot be used for DSC measurements on certain materials, e.g. for steels in the high temperature range. The steel loses alloying components with increasing temperature which leads to a surface corrosion of the platinum crucible or can form easily fusible alloys which destroys the crucible. In [1] measures were discussed how to use the advantages of both crucible materials ($A1_2O_3$ and Pt) in order to obtain good experimental results. A high emissivity improves the heat transfer between the sample crucible and the reference crucibles among other things. This results in a decrease in the DSC signal. Therefore, the use of a radiation

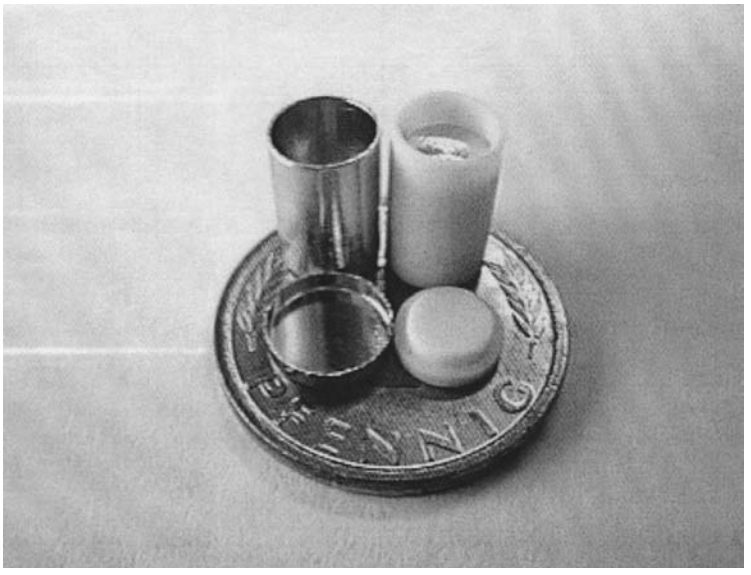

Fig. 4. Crucibles with cover used for DSC measurements; left: platinum, right: Al_2O_3.

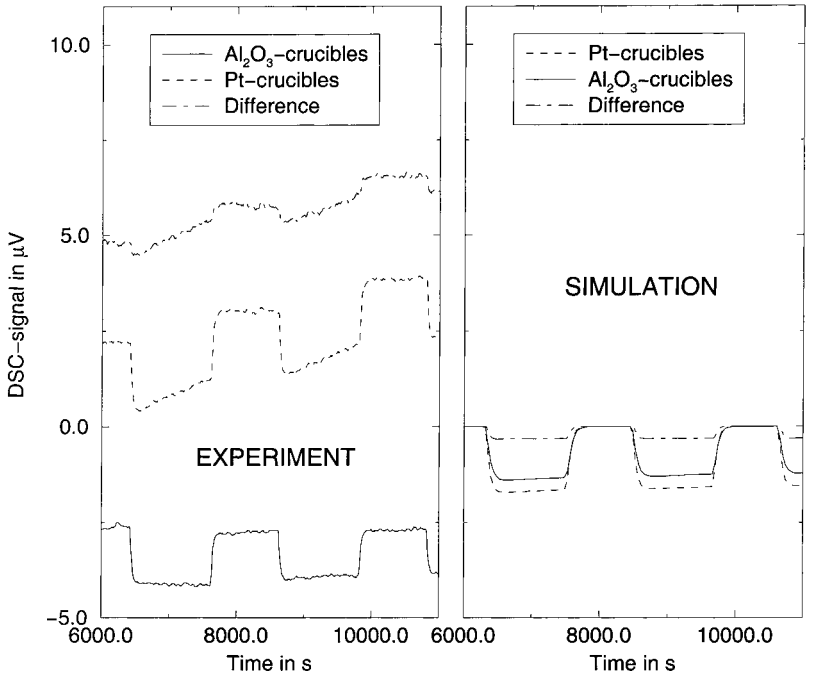

Fig. 5. Comparison of the DSC signals for different crucible materials and comparison with the simulation (Pt–sample cylinder, helium atmosphere, heating rate 5 K/min).

protection in the high temperature range is appropriate when Al_2O_3 crucibles are used.

The influences of a change in emissivity or thermal conductivity can be simulated with the proposed model. Also, the influence of the advantageous use of $A1_2O_3$ crucibles inside platinum crucibles can be shown by use of the model. In Fig. 5, the comparison of the experimentally determined DSC signals with

the simulated ones is presented as an example. A platinum cylinder was used as the sample. When using platinum crucibles, the signal changes are larger than those achieved with Al_2O_3 crucibles. The presented measured DSC signal (difference of the plate temperatures) with the transition from the plateau to the constant heating rate and vice versa can be reproduced by the model (Fig. 5, right). In Fig. 5 (left) it can be seen that the drift of the base line is also dependent on the crucible material. For simulation full symmetry of the sample and reference side is assumed. Therefore, the DSC signal was held at a value of 0 in the plateau phases for both crucible materials (Fig. 5, right). However, consideration of the base line drift is possible without much efforts.

For the investigation of the response of the temperature level to the signal change, experiments with a cascade-type heating were carried out in a wide temperature range. In the lower part of Fig. 6, the temperature program used of 700–1400°C with 100 K steps is shown. The simulated and experimental determined DSC signals are presented in the upper part of Fig. 6. It can be seen that the signal changes decrease with increasing temperature, although the specific heat capacity of platinum increases by more than 10% in this temperature range. The reasons for this are the changing conditions for the heat transfer. This effect can be reproduced by the simulation with a high accuracy.

It can be concluded that the simulated temperatures $T_i(t)$ reflect changes of the heat flow between the subsystems well. Thus, the influence of the particular thermal resistances and the selected heating rates can be predicted. In addition, the estimation of the necessary length of the plateau phases is simplified. The signal behavior can be simulated in dependence on:

the crucible selection ($A1_2O_3$, Pt),
the inert gas (He, Ar),
the thermalphysical properties of the sample (λ, c_p, ρ, ϵ),
the geometry of the sample (dimensions, surface quality),
the selected temperature program.

4. Conclusion

After adapting the model parameters to the appropriate DSC plate transducer, an efficient model is

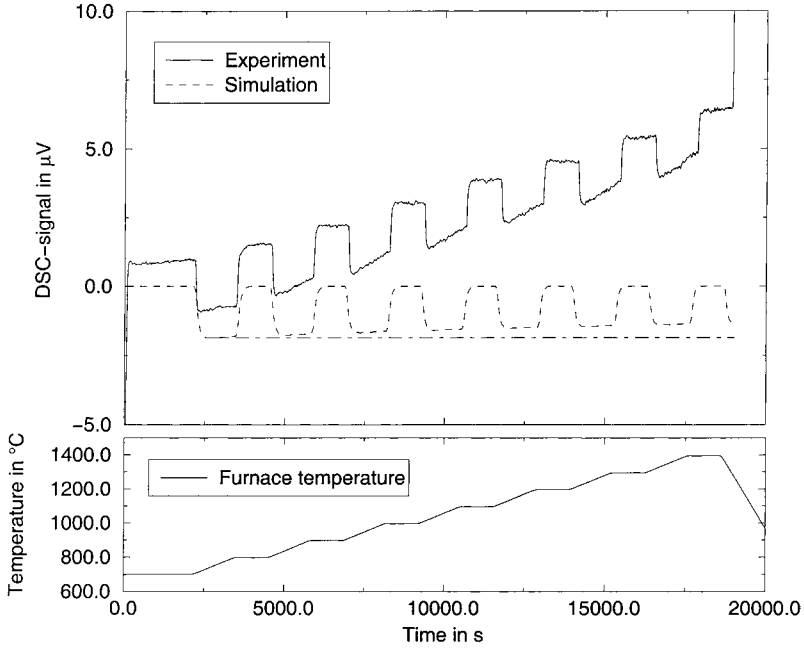

Fig. 6. Comparison of the DSC signals in the range of 700–1400°C (Pt–crucible, Pt–sample cylinder, helium atmosphere, heating rate 5 K/min).

available for the numerical analysis of DSC measurements. The influences of the particular thermal resistances on the signal measured can be interpreted well. Thus, conclusions can be derived for an optimum planing of experiments as well as for the interpretation of experimental results. The method is also suitable for the description of special procedures, like the temperature-modulated DSC. In addition, asymmetries can be simulated which lead to a drift of the base line. Further simulation results and proposals for an improved experiment planing, especially for the consideration of the influence of the inert gas as well as the properties and geometry of the sample, will be presented in a paper which is in preparation.

5. Nomenclature

A	heat transfer surface
Bi	Biot number: $\mathrm{Bi} = \alpha \cdot l_{\mathrm{char}}/\lambda$, l_{char} characteristic length
c	specific heat capacity
m	mass
Nu	Nusselt number
Q	heat
$\dot{Q}$	heat flow
R	thermal resistance
s	distance
T	temperature
t	time
U	internal energy
$\dot{V}$	flow rate
α	heat transfer coefficient
β	heating rate
ϵ	emissivity
λ	thermal conductivity
σ_s	Stefan–Boltzmann constant

Indices

eff	effective
conv	convective
gas	gas
i	index for subsystem
j	index for subsystem
o	furnace
p	sample side
pl	plate
pr	sample
	cross section
q	
r	reference side
rough	roughness
tb	crucible ground
tm	crucible coat

References

[1] A. Lindemann, J. Al-Karawi, J. Schmidt, Thermal analytical study of steels at high temperature including the range of melting, Thermochimica Acta 310 (1998) 133–140.
[2] K. Kanari, T. Ozawa, Simulation of temperature modulated DSC of temperature dependent heat capacity, Thermochimica Acta 304/305 (1997) 201–207.
[3] K. Kanari, T. Ozawa, Simulation of temperature modulated DSC of transitions represented by abrupt changes in heat capacity, Journal of Thermal Analysis 94 (1997) 979–989.
[4] G.W.H. Höhne, N.B. Shenogina, Finite-element calculations on the behaviour of a DSC in temperature-modulated mode, Thermochimica Acta 310 (1998) 47–51.
[5] B. Chowdhry, S. Leharne, Simulation and analysis of differential scanning calorimetry output: protein unfolding studies 1, Journal of Chemical Education 74 (1997) 236–240.
[6] VDI-Warmeatlas, Berechnungsblätter für den Wärmeiubergang, 8. Auflage, VDI-Verlag, Düsseldorf, 1998.
[7] G. Engeln-Müllges, F. Reutter, Numerik-Algorithmen, Entscheidungshilfe zur Auswahl und Nutzung, 8. Auflage, VDI-Verlag, Dusseldorf, 1996.